Impact of spectral coupling between urban atmosphere and sky boundary conditions in a street canyon

Félix Schmitt, Mathieu Galtier, Lucie Merlier, Etienne Vergnault, Frédéric André

Impact of spectral coupling between urban atmosphere and sky boundary conditions in a street canyon

Félix Schmitt[a], Mathieu Galtier[a], Lucie Merlier[b], Etienne Vergnault[b], Frédéric André[c]

[a] *Univ. Lyon, INSA Lyon, CNRS, CETHIL, UMR5008, Villeurbanne, F-69621, France*
[b] *Univ. Lyon, UCBL, INSA Lyon, CNRS, CETHIL, UMR5008, Villeurbanne, F-69621, France*
[c] *Univ. Lille, CNRS, LOA, UMR8518, Villeneuve d'Ascq, F-59655, France*

Abstract

Most radiative transfer models developed for the analysis of urban configurations consider a transparent urban atmosphere and gray sky conditions. The aim of the present work is to investigate these assumptions, focusing on the longwave domain. For this purpose, reference Line-by-Line Monte-Carlo calculations are first performed. A more efficient radiative transfer model based on the Finite Volume Method and SLW modeling is also developed to treat several street canyon configurations. The aspect ratio of the street canyon, a parameter frequently encountered in urban scenarios, is considered for the analysis. It is shown that, in most cases, real urban problems need to take into account a non-gray participating atmosphere within the streets, together with its spectral coupling with the non-gray sky downward radiation, to provide accurate net fluxes on urban surfaces and volumetric radiative powers in the urban atmosphere.

Keywords: Radiative transfer, Urban environment, Street canyon, Participating medium, Monte-Carlo, SLW model, Finite volume method

1. Introduction

Urban areas are characterized by artificial surfaces and differ from rural areas in their structure, fabric, cover and metabolism. These urban features involve specific and complex thermo-physical interactions [1]. At microscale, the variability and heterogeneity of urban forms lead to the existence of a multitude of local microclimatic conditions that develop within the urban canopy layer, most of the time responsible for overheating compared to rural environments [2, 3, 4, 5]. Given that these effects will be increasingly critical in the next decades due to more frequent and intense heat waves [6], the so-called and well-known Urban Heat Island phenomenon is gaining more and more attention. Indeed, it has serious impacts on the citizen's comfort and health [7, 8] and on the cooling energy demand of buildings [9], especially in summer.

Solar radiation (shortwave spectral range) and infrared radiation (longwave spectral range) play a significant role in the overall energy balance in urban zones and the resulting urban microclimates [10]. In this context, detailed and reliable radiative simulations in urban environments are needed to better evaluate adaptation strategies for cities [11, 12]. More specifically, longwave radiation is partly responsible for the cooling of urban surfaces during nighttime and can even become the main factor affecting their heat balance under low wind conditions. During hot periods, an accurate estimation of longwave radiation is therefore of primary importance to suggest relevant heat attenuation strategies for urban areas. At a larger scale, radiative exchanges between urban surfaces and the atmosphere significantly impact the regional climate and, consequently, need to be estimated accurately in mesoscale weather and climate models [13].

The impact of urban morphology, fraction of vegetation or longwave radiative properties of the building materials on the longwave radiative budget of the urban canopy layer and their role in favoring urban overheating have been widely studied (see *e.g.* Ref. [5] for an extended review). However, the impact of the interactions between longwave radiation and the participating urban atmosphere has been assessed only sparsely. To the best of the authors' knowledge, to date, most of the radiative models that have been developed for studying radiative transfer in urban areas almost systematically consider the urban

atmosphere as transparent. Nevertheless, some works have emphasized the need to better characterize the effects of longwave absorption in urban contexts, since they can be significant. Verseghy and Munro [14] investigated numerically the influence of the participating atmosphere within a building courtyard. Neglecting the absorption and emission by the air colder than the walls resulted in overestimating the incident longwave flux by up to 10 W.m^{-2} on the building walls for clear-sky conditions. Hogan [15] performed longwave simulations in an urban canopy layer with a mean wall-to-wall distance of 50 m under Mid-Latitude Summer conditions using a discrete-ordinate method coupled with a statistical description of the urban geometry capable of explicitly representing gaseous absorption and emission of the atmosphere within the canopy layer. When the walls and ground facets are 10 °C hotter than the air, results showed that for a mean building height going from 10 to 50 m, taking the absorption by the urban atmosphere into account results in a decrease in the mean absorbed flux by the vertical walls that ranges from 5.7 to 44.0 W.m^{-2} compared to the case where the urban atmosphere is assumed transparent. On the basis of radiative simulations carried out with a Monte-Carlo-based urban radiative solver in explicit and realistic urban scenes, Schoetter et al. [16] also highlighted the strong impact of the interactions between longwave radiation and clear air in the urban canopy layer on the urban radiative budget, especially for urban zones with tall buildings and large differences between skin surface temperatures and air temperature. Thermo-radiative conditions at the microscale in an urban block formed by several buildings with realistic shapes were studied numerically by Wang [17] during a period of five consecutive days. A significant impact of the interactions between the longwave radiation and the air was noticed in the scene on the net wall fluxes and the time evolution of the surface temperatures compared to cases for which these interactions were neglected. However, the author drew attention to the fact that a proper and rigorous spectral treatment of the boundary conditions at the sky boundary should be carried out, otherwise significant errors could be made on the computed radiative quantities.

From an aeraulic perspective, with a light ambient wind, the airflow structures and turbulent features can be significantly influenced by buoyancy forces driven by temperature gradients between building walls and urban atmosphere. The radiative volumetric power generated by the interactions between longwave radiation and this atmosphere can therefore potentially affect the airflow within the streets, in a similar way to what has been observed in *e.g.* differentially heated cavities for turbulent flows of participating gas mixtures [18, 19, 20].

The purpose of the present paper is thus to investigate further the errors on the radiative fluxes and volumetric powers that can be made when considering a transparent atmosphere within a street canyon. This is achieved by analyzing the influence of the high spectral resolution coupling between the non-gray longwave radiation coming from the sky and the non-gray absorption by the atmosphere within the urban canopy layer. Additionally, this work aims to provide an approximate model associated with an efficient solver to accurately account for spectral interactions between the participating urban atmosphere and the sky boundary conditions. The proposed approach is used to evaluate the impact of these errors on the global heat exchanges between surfaces and their surrounding environment, impacting their cooling rate.

The paper is structured as follows. In Section 2, a Monte-Carlo code is used to achieve line-by-line calculations and evaluate the radiative net fluxes and volumetric powers in a given street canyon configuration. The discrepancies induced by gray or non-gray sky models and by transparent or participating urban atmospheres are discussed in detail. Then, in Section 3, an approximate method based on the Finite Volume Method and on SLW modeling is proposed to treat similar configurations in a more computationally efficient way. Finally, in Section 4, the numerical method described in Section 3 is applied for a quantitative analysis of the errors associated with a transparent atmosphere assumption, for various street aspect ratios.

2. Overall impact of atmospheric absorption/emission on longwave radiation in a street canyon

2.1. Description of the considered street canyon

The longwave radiative simulations are carried out in a standard two-dimensional street canyon configuration, as depicted in Figure 1. This street (infinite in the y direction) has a height H of 21 m and a width W of 14 m (*i.e.* an aspect ratio H/W of 1.5), thus representative of a compact mid-rise urban setting

[3]. Both the walls and the ground are assumed to be gray with an emissivity $\epsilon_A = \epsilon_B = \epsilon_g$ of 0.9, and isotropically emitting in the longwave range. The temperatures of the walls A and B and the ground are $T_A = 25$ °C, $T_B = 35$ °C and $T_g = 25$ °C respectively.

Two sky boundary condition models are considered, defining the boundary condition at the interface between the street canyon and the atmosphere located at the top of the street canyon. The first one, from now on referred to as *gray sky*, treats the sky as a gray and isotropic surface, as usually assumed in radiative transfer models in urban configurations. For the second sky model, from now on referred to as *spectral sky*, a line-by-line (LBL) spectrum has been generated using the HITRAN2020 molecular spectroscopic database [21] to model the downward longwave spectral intensities coming from the sky at the top of the street canyon, noted $I_{\eta\downarrow,\mathrm{sky}}$, assuming a standard Mid-Latitude Summer (MLS) atmosphere [22]. The MLS profiles give the temperature, pressure and mole fractions of water vapor, CO_2, O_3, N_2O, CO, CH_4 and O_2 at different altitudes. This LBL spectrum has been calculated at a spectral resolution of 5×10^{-3} cm^{-1} and using Voigt line profiles. Scattering phenomena and aerosols have been neglected in these LBL calculations. For propagation directions close to the horizon, the total optical thickness of terrestrial atmosphere becomes important, so that the spectral emission is more important at wavenumbers where the atmosphere is usually weakly emitting (mainly in the atmospheric window between 750 cm^{-1} and 1250 cm^{-1}). Consequently, the downward intensity spectrum depends on the incident angle, especially for angles higher than 60° under clear sky conditions. A field measurement campaign in Anglet (France) has revealed that the assumption of isotropic downward longwave intensities implied an underestimation of 11 W.m^{-2} of the modeled irradiance on a non-obstructed vertical North-facing wall with a clear sky compared to the measured irradiance during daytime (163 W.m^{-2}) [23], which corresponds to a relative difference of -6.8 %. This underestimation is expected to be lower on a horizontal surface. In the case of urban environments, the impact of the isotropic sky approximation is attenuated by the obstruction of the sky by buildings, especially in dense

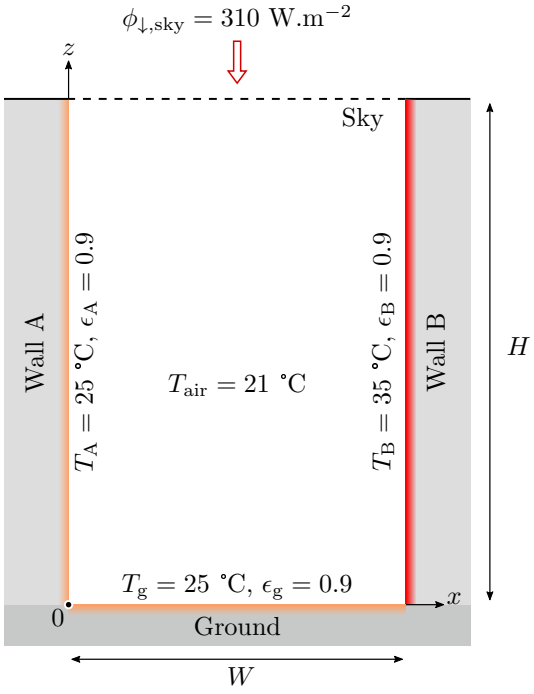

Figure 1: Configuration and size of the street canyon, infinitely long in the y direction. The gray emissivities ε and temperatures T of each wall are specified, along with the temperature of the urban atmosphere and the value of the downward longwave flux coming from the sky $\phi_{\downarrow,\mathrm{sky}}$.

urban areas where the sky-view-factors of surfaces are lower. The errors induced by this assumption will therefore be essentially localized on the upper part of vertical building facades. For the remainder of this study, the downward spectral intensity $I_{\eta\downarrow,sky}$ will therefore be considered uniform in all directions as a first approximation, its value being taken as an angular average of the directional intensities. The resulting spectrum of the sky downward isotropic intensity is depicted in Figure 2a. The value of the corresponding total downward flux (integrated over the entire longwave range) is $\phi_{\downarrow,\mathrm{sky}} = 310$ W.m^{-2}. For comparison purposes, this integrated value is also taken for the gray sky model, leading to an effective emissivity of 0.73 for a temperature of 21 °C.

The state of the urban atmosphere within the street canyon is identical to the state specified in the MLS profiles at the ground level. This urban atmosphere is assumed to be composed of clear air only and is called from now on *urban air*. In particular, aerosols and scattering phenomena inside the street canyon have been neglected. Its temperature, pressure and species mole fractions, uniform within the street canyon, are: $T_{\mathrm{air}} = 21$ °C, $p = 1$ atm, $x_{\mathrm{H_2O}} = 1.88$ %, $x_{\mathrm{CO_2}} = 417$ ppm, $x_{\mathrm{O_3}} = 0.03$ ppm, $x_{\mathrm{N_2O}} = 0.32$ ppm, $x_{\mathrm{CH_4}} = 1.7$ ppm, $x_{\mathrm{CO}} = 0.15$ ppm and $x_{\mathrm{O_2}} = 20.9$ %. In the same way as the sky downward intensity, a LBL absorption spectrum has been produced for the urban air. This spectrum is depicted in Figure 2b. It can be seen from Figure 2b that the urban air can hardly be considered transparent, except in the atmospheric transparency zone (window from 750 cm^{-1} to 1250 cm^{-1}), clearly visible in Figure 2a.

Three different cases, corresponding to different treatments of the spectral attributes of the urban air and the sky downward intensities, are considered:

- *Case 1*: a transparent urban air combined with the gray sky model (the most widely used assumptions for studying urban configurations);
- *Case 2*: a non-gray participating urban air combined with the gray sky model;
- *Case 3*: a non-gray participating urban air combined with the spectral sky model.

It can be noticed that for Case 1, using either the gray sky or the spectral sky model is strictly equivalent, since the urban air is transparent, the total sky fluxes are identical and the walls and the ground are assumed as gray.

2.2. Effects of the different models on the surface fluxes

In this section, the radiative transfer equation is solved in the street canyon using a standard backward Monte-Carlo (MC) algorithm. For the spectral integration, wavenumbers are randomly sampled according to Planck's distribution at the maximum temperature encountered in the considered configuration, *i.e.* 35 °C. At each location, where the net fluxes on the walls or the volumetric radiative powers in the urban air are evaluated, a full MC simulation using 10^8 realizations has been performed.

In the following sections, the net flux on a wall, noted Φ_{w} with subscript "w" referring either to wall A (subscript "A"), wall B (subscript "B") or the ground (subscript "g"), are defined as the absorbed flux minus the emitted flux:

$$\Phi_{\mathrm{w}} = \epsilon_{\mathrm{w}} \left(E_{\mathrm{w}} - \sigma T_{\mathrm{w}}^4 \right) \tag{1}$$

In Equation 1, the irradiance E_{w}, *i.e.* the flux received by the wall, is solved by the radiative solver.

The net flux on the sky boundary, noted Φ_{sky}, is defined as the flux leaving the street (noted $\Phi_{\uparrow,\mathrm{sky}}$) minus that entering it (corresponding to the total downward flux $\Phi_{\downarrow,\mathrm{sky}}$ presented in the previous section):

$$\Phi_{\mathrm{sky}} = \Phi_{\uparrow,\mathrm{sky}} - \Phi_{\downarrow,\mathrm{sky}} \tag{2}$$

In Equation 2, $\Phi_{\uparrow,\mathrm{sky}}$ is solved by the radiative solver.

The net fluxes computed with the MC-LBL solver for each case, at several locations on the four boundaries (walls A and B, ground and sky), are depicted in Figure 3. As each calculation accounts for 10^8 independent MC samples, standard deviations are negligible (in the order of 10^{-2} W.m^{-2}) and are thus not depicted on the figure. It can be seen that the three different cases lead to significant differences in net fluxes (up

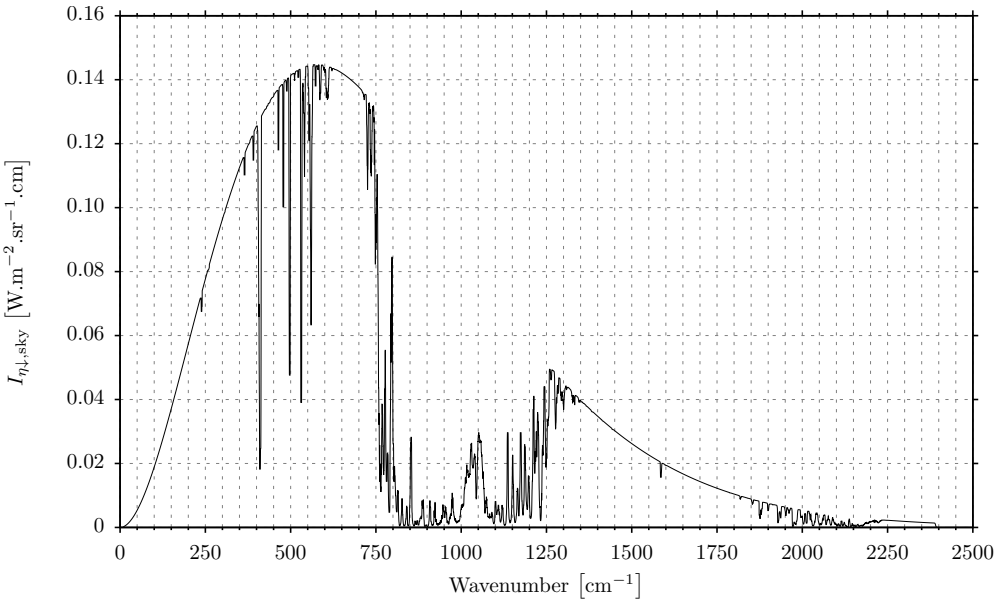

(a) Sky downward isotropic intensity $I_{\eta\downarrow,sky}$

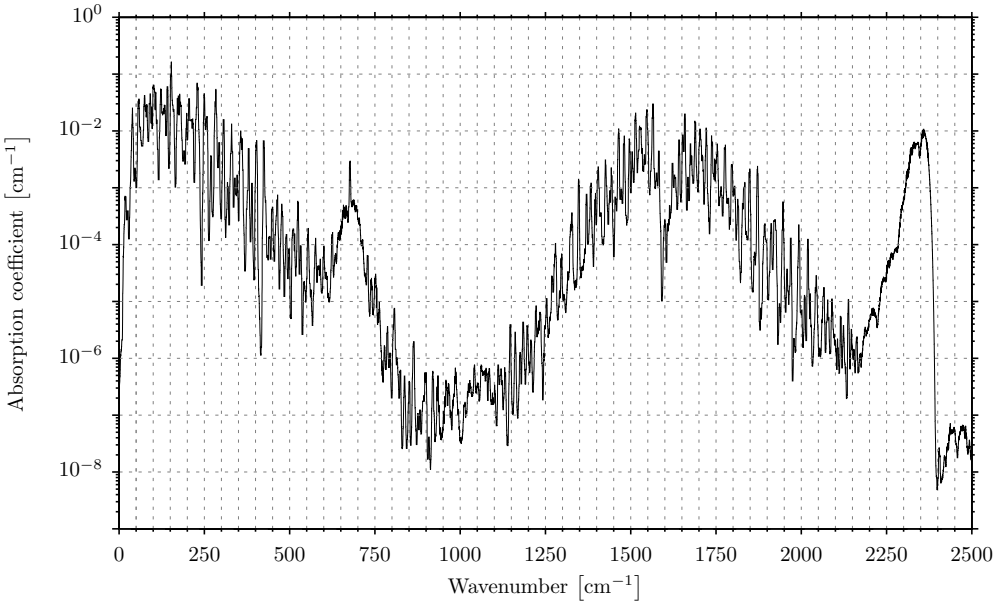

(b) Absorption coefficient

Figure 2: Spectra of the sky downward isotropic intensity $I_{\eta\downarrow,\mathrm{sky}}$ and of the absorption coefficient at the ground level (generated with MLS atmospheric profiles). The spectra are smoothed by a sliding median with a window of 5 cm^{-1}.

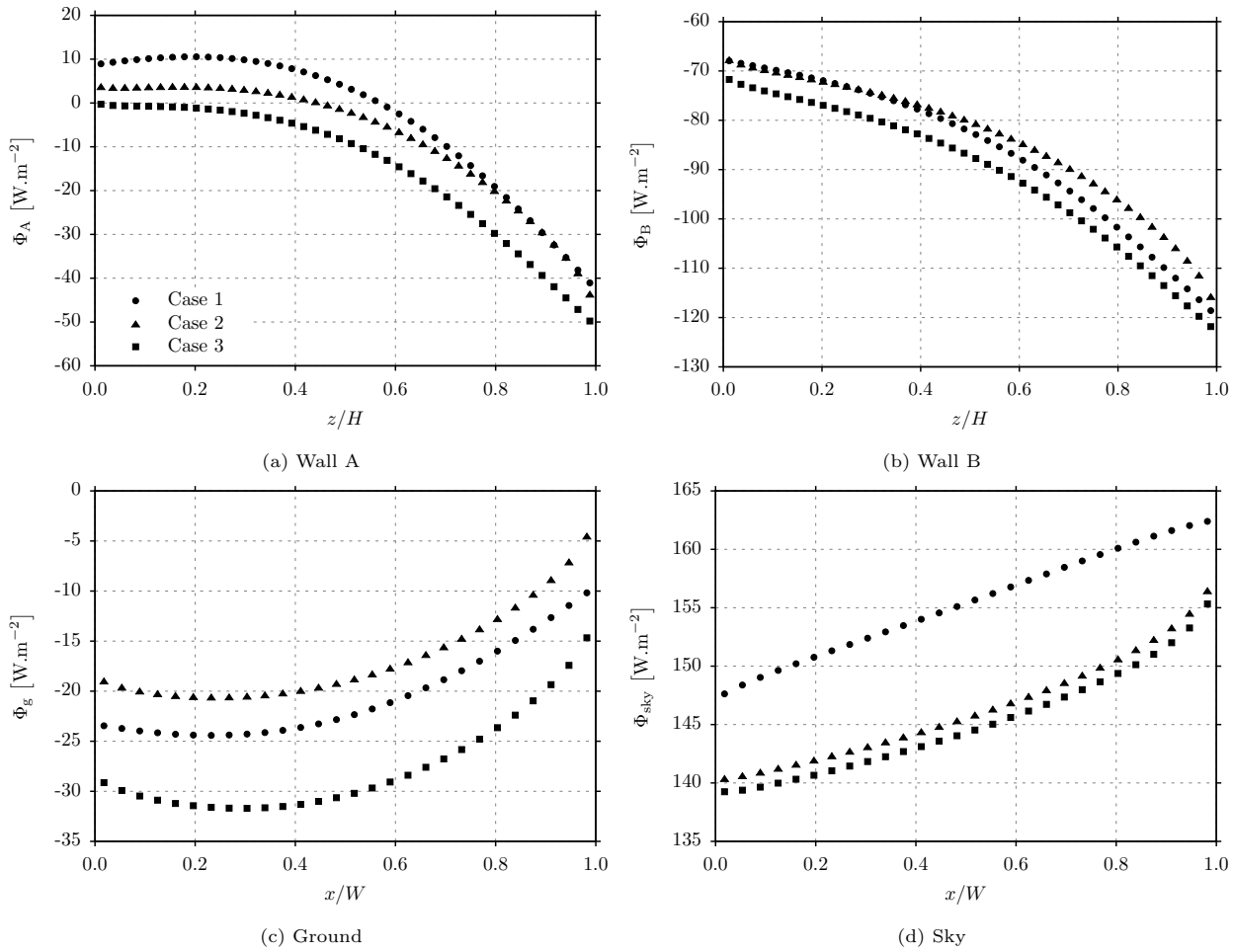

(a) Wall A

(b) Wall B

(c) Ground

(d) Sky

Figure 3: Net longwave fluxes on the street canyon walls, Φ_w, and at the sky boundary, Φ_{sky}, for the three selected cases. The x-axis represents the vertical location for walls A and B (3a and 3b) and the horizontal location for the ground (3c) and the sky (3d), as defined on Figure 1. Case 1: Transparent - Gray sky, Case 2: Participating - Gray sky, Case 3: Participating - Spectral sky.

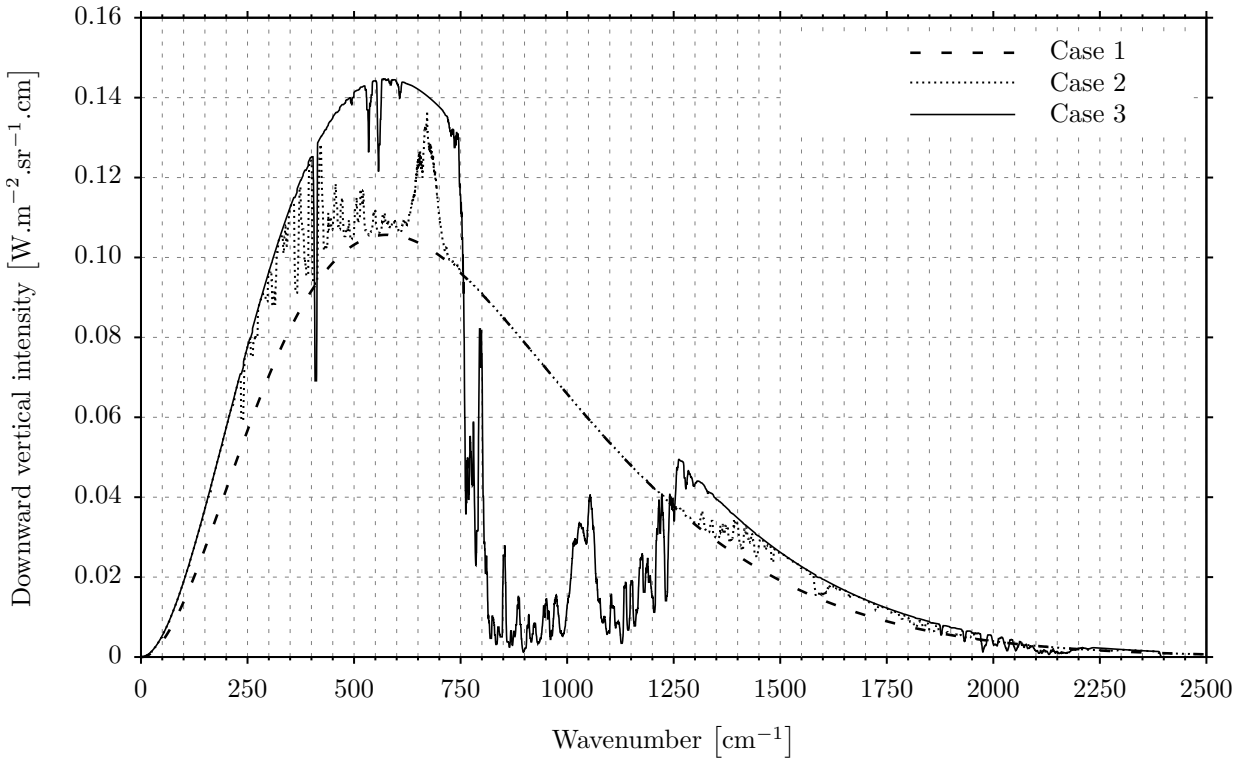

Figure 4: Spectra of the downward vertical intensity in the canyon at the ground level for the three considered cases. The spectra are smoothed by a sliding median with a window of 10 cm^{-1}. Case 1: Transparent - Gray sky, Case 2: Participating - Gray sky, Case 3: Participating - Spectral sky.

to 12 W.m^{-2}). To illustrate the reasons for these discrepancies, Figure 4 shows the spectral distribution of the downward intensity at the ground level in a vertical direction (ensuring that the incoming radiation is not intercepted by the walls) for the three cases. In the transparent case (Case 1), the spectral distribution of the sky boundary condition is obviously preserved during the propagation of radiation in the urban air: the downward intensity spectra at the top and bottom of the street canyon are identical. The same applies to Case 3 with the participating urban air and the spectral sky. The continuity of the thermo-radiative properties between the MLS atmosphere - that led to the sky downward intensity spectrum - and those of the urban air within the street ensures that, over a distance of a few dozen meters (short compared to the characteristic dimensions of the atmosphere), the intensity spectrum will be almost unaltered. In other words, the absorption by the urban air almost totally compensates for its emission. However, in Case 2 (participating urban air and gray sky), the incoming gray radiation located in the atmospheric window $\left[750\text{ cm}^{-1} - 1250\text{ cm}^{-1}\right]$ undergoes no change as it propagates through the urban air, since the absorptivity of the air in this region is virtually zero. In addition, a volumetric emission surplus is contributed by the urban air in the most participating spectral regions (below 750 cm^{-1} and above 1250 cm^{-1}) as radiation propagates in the urban air, because the incoming gray intensities have been underestimated in this region to ensure a given total flux of 310 W.m^{-2}. This is why, as radiation propagates vertically, the intensity values increase in this spectral band and the shape of the spectrum approaches the shape of the spectrum obtained with the atmospheric transfer model, while in the atmospheric window the intensity remains unchanged. Consequently, the spectral discontinuity at the sky interface due to the gray sky modeling induces an overestimation of the total downward intensities, resulting in an overestimation of the net fluxes on each wall for Case 2 compared to Case 3 as can be seen in Figure 3. Moreover, these differences are higher at the wall locations presenting higher sky-view-factors, *i.e.* in the upper part of the walls A and B and in the

central zone of the ground as evidenced in Figure 3.

These results lead to two main conclusions: 1/ it is important to take into account the participating nature of the urban air in the street canyon: significant differences were observed between the transparent (Case 1) and the participating with spectral sky (Case 3) models. These absolute differences - averaged over each boundary - are respectively of 11.3 $W.m^{-2}$ for the wall A, 4.5 $W.m^{-2}$ for the wall B, 7.2 $W.m^{-2}$ for the ground and 10.2 $W.m^{-2}$ for the sky, when comparing Case 3 to Case 1. The impact of such deviations on the heat balance of these surfaces is not negligible, as will be shown in Section 4. These differences are expected to increase when the temperature differences between the canyon surfaces and the air increase, because of an enhanced longwave attenuation of gray surface radiation within the urban air. Consequently, usual urban radiative models, that treat the urban atmosphere as transparent, are likely to give incorrect longwave fluxes on urban surfaces when temperature gradients within the canopy are significant; 2/ taking into account the participating nature of the urban air implies defining sky boundary conditions that are spectrally described and ensuring the continuity of the thermo-radiative properties between the urban air and the atmospheric emission modeling. As shown in Figure 3, the assumption of a gray sky associated with a participating urban air leads indeed to a significant overestimation of the net fluxes.

2.3. Effects of the different models on the volumetric radiative powers

In the following sections, the volumetric radiative power in the urban air, noted P_{air}, is defined as the longwave power absorbed minus the longwave power emitted by the urban air, and corresponds to the opposite of the divergence of the radiative flux vector in the urban air ($\boldsymbol{\nabla} \cdot \mathbf{q}_{\text{r}}$) which is solved by the radiative solver:

$$P_{\text{air}} = -\boldsymbol{\nabla} \cdot \mathbf{q}_{\text{r}} \tag{3}$$

The volumetric radiative power fields calculated with the MC-LBL algorithm are shown in Figure 5 for Cases 2 and 3, where the urban air is participating. These powers are null for Case 1 with a transparent urban air. In both cases, the volumetric radiative power is low at the center of the street canyon, with values below 1 $W.m^{-3}$. It can also be observed that the main effects of the longwave radiation absorption on the energy budget of the urban air is highly localized. The absorption of the radiation emitted by the walls occurs mainly in the first few meters traveled within the urban air, where volumetric radiative powers can reach 10 $W.m^{-3}$ near the hottest wall (wall B). These localized heat sources within the urban air may have some effects on air convection and temperature.

As previously discussed, one can also note that in Case 3 (with a participating urban air and the spectral sky, Figure 5b), the volumetric radiative power shows no discontinuity near the sky boundary, in line with the continuous spectral coupling associated with the spectral processing of the sky. In Case 2. With a participating urban air and the gray sky, Figure 5a), a strong discontinuity in the volumetric radiative power is visible near the sky boundary, with values as high as -16 $W.m^{-3}$ linked to the enhancement of the incoming downward sky intensities as discussed in the previous section, *i.e.* the longwave emission by the urban air locally greater than the absorption. As can be seen on Figure 5c, this discontinuity in Case 2 induces negative differences in the canyon compared to Case 3. These differences are particularly strong in a zone near the sky boundary and attenuate deeper in the canyon, approaching zero in the lower part.

3. Description of an efficient approximate radiative transfer model

In operational situations, the MC-LBL method described in the previous sections may not be recommended for coupled simulations due to its high CPU cost. The aim of the present section is thus to develop a faster though accurate model for handling this type of simulations.

3.1. Modeling the radiative properties of the urban air and the sky

As shown in Section 2, the main difficulty in dealing with radiative transfer in the urban canopy layer consists of the proper treatment of the relationships, that occur at high spectral resolution, between the non-gray sky downward radiation and the urban air located inside the street canyon. There exist several

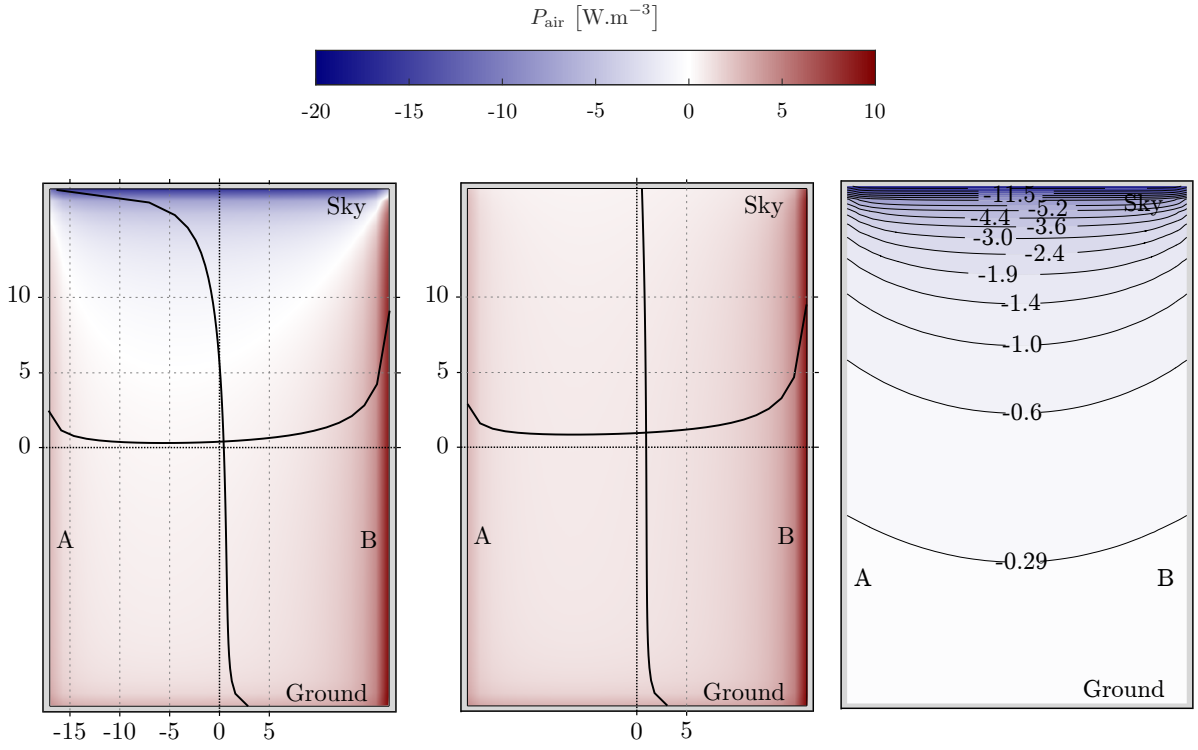

(a) Case 2: Part. - Gray sky

(b) Case 3: Part. - Spectral sky

(c) Diff. betw. Case 2 and 3

Figure 5: Volumetric radiative power, P_{air}, obtained within the air in the street, depending on the sky treatment used. The color palette is used to give the values on the 2D plane of the street canyon, identical to the plane shown in Figure 1. Figures 5a and 5b give the values of P_{air} in Case 2 and Case 3 respectively, and Figure 5c gives the contours of differences in the values in Case 2 with respect to Case 3.
In addition, the two curves shown on Figures 5a and 5b give the value of this power on the vertical line at $x/H = 0.5$ (bottom scale) and on the horizontal line at $z/H = 0.5$ (left scale).

methods to treat radiative transfer in gaseous media. The most widely spread methods are presently the Weighted-Sum-of-Gray-Gases (WSGG) [24, 25], Full-spectrum k-distribution (FSK) [26, 27] and Spectral Line Weighted-sum-of-gray-gases (SLW) [28, 29, 30, 31, 32, 33] approaches. Here, the SLW model was selected. In order to formulate a global absorption method allowing this kind of treatment, let us consider a radiation path that comes from the sky and propagates in a downward direction (the corresponding source term is written S_ν). Its integral over the full spectrum is $S = \int_0^{+\infty} S_\nu \, d\nu$. When this radiation travels a distance L inside the urban air where the corresponding absorption coefficient is κ_ν, the amount of radiation absorbed by the urban air can be written in terms of an effective absorptivity α_{eff} defined as:

$$\alpha_{\text{eff}} = \frac{1}{S} \cdot \int_0^{+\infty} \left(1 - e^{-\kappa_\nu L}\right) S_\nu \, d\nu \tag{4}$$

Equation 4 was approximated in the present work by:

1/ generating a discrete set (gray gases) of values of absorption coefficients in the urban air using the Absorption Line Blackbody Distribution Function (ALBDF) defined at the air temperature, pressure and species mole fraction inside the street canyon, together with a Gauss-Legendre quadrature. The corresponding values of the urban air absorption coefficients are then k_i^{air}, $i = 1, \cdots, N$ where N is the order of the Gauss-Legendre quadrature (k_0^{air} is taken equal to 0). Supplemental values of the absorption coefficients, $\tilde{k}_i^{\text{air}}$, $i = 0, \cdots, N$, are also generated in the same way as in SLW models [34, 35].

2/ using the previous sets of absorption coefficients to approximate Equation 4 as:

$$\alpha_{\text{eff}} = \sum_{i=0}^{N} \left(1 - e^{-k_i^{\text{air}} L}\right) \cdot \left[F\left(\tilde{k}_i^{\text{air}}\right) - F\left(\tilde{k}_{i-1}^{\text{air}}\right)\right] \tag{5}$$

where

$$F(k) = \frac{1}{S} \cdot \int_0^{+\infty} H\left(k - \kappa_\nu\right) S_\nu \, d\nu \tag{6}$$

and H is the Heaviside function. F thus represents the fraction of the source term S_ν averaged over the set of wavenumbers where the absorption coefficient of the urban air takes a value lower than k. F plays the same role as a usual ALBDF, but is defined in terms of the source term S_ν instead of the more usual Planck's distribution $I_{\text{b},\nu}$ at a given source temperature. In the literature [36, 37], functions of the type of F as given by Equation 6 are referred to as Absorption Line Distribution Functions (ALDF). As S_ν is strictly positive, as shown in Figure 2a, one can easily verify that Equation 6 defines a proper distribution function of absorption coefficients [38]. The difference $F\left(\tilde{k}_i^{\text{air}}\right) - F\left(\tilde{k}_{i-1}^{\text{air}}\right)$ that appears in Equation 5 thus represents the fraction of the source term S_ν averaged over the set of wavenumbers where the absorption coefficient of the urban air is close to k_i^{air}. $F\left(\tilde{k}_i^{\text{air}}\right) - F\left(\tilde{k}_{i-1}^{\text{air}}\right)$ allows defining the weights needed to specify the sky boundary conditions. The weights at the walls are defined in terms of the differences $F\left(\tilde{k}_i^{\text{air}}, T_{\text{w}}\right) - F\left(\tilde{k}_{i-1}^{\text{air}}, T_{\text{w}}\right)$ where

$$F\left(k, T_{\text{w}}\right) = \frac{1}{I_{\text{b}}\left(T_{\text{w}}\right)} \int_0^{+\infty} H(k - \kappa_\nu) I_{\text{b},\nu}(T_{\text{w}}) \, d\nu \tag{7}$$

are usual ALBDFs at the wall temperature T_{w} (either T_{A}, T_{B} or T_{g}). This formalism complies with the method used in SLW modeling [34]. Consequently, this radiative absorption model is from now on referred to as *SLW model*, even if it is formulated in k-form.

3.2. Resolution of the radiative transfer equation with the finite volume method

A finite volume method (FVM)-based radiative solver [39, 40], much faster than the MC method described in Section 2 with regard to chosen parameters and implementations, was developed and associated with the SLW model to perform the radiative transfer calculations. A uniform Cartesian spatial mesh along with a first-order forward spatial differencing scheme (also called step scheme) and the so-called FT_n angular discretization scheme [41] were used. A preliminary sensitivity analysis has been carried out to select suitable spatial and angular meshes for the FVM in the street canyon configuration with transparent urban air (Case 1). Excellent agreement with the MC results has been obtained for a 0.25 m uniform spatial mesh combined with 3248 control angles, based on comparisons of the net wall fluxes. This mesh has thus been selected for all the subsequent simulations. Moreover, a sensitivity analysis on the number of gray gases of the SLW method has been carried out using respectively 5, 10 and 15 gray gases (including a clear gas). Tables 1 and 2 gather the mean absolute errors (MAE) and the root-mean-square errors (RMSE) on the net fluxes and on the volumetric radiative powers respectively, in comparison to MC-LBL results. These errors have been evaluated for equally spaced locations with a 0.25 m spatial step on every boundaries for the net fluxes and in the canyon air for the volumetric radiative powers. Concerning the net fluxes (Table 1), the errors are small in comparison with their values on the boundaries (see Figure 3), and do not vary when the number of gray gases increases from 5 to 15. Concerning the volumetric radiative powers (Table 2), the MAE and RMSE are equal to 0.10 W.m^{-3} and 0.24 W.m^{-3} respectively with 10 gray gases, against 0.16 W.m^{-3} and 0.27 W.m^{-3} respectively with 5 gray gases, which represents a noticeable enhancement in light of the order of magnitude of these powers within the air in the street (below 10 W.m^{-3} as seen in Section 2.3). Because using 15 gray gases instead of 10 does not allow to significantly reduce these errors, 10 gray gases were used for the subsequent simulations.

Figure 6 shows the deviations of the net fluxes computed by the FVM-SLW solver with 10 gray gases from those computed with the MC-LBL solver, for the three cases defined in Section 2.1. According to

Table 1: Mean absolute errors (MAE) and root-mean-square errors (RMSE) on the net fluxes for different numbers of gray gases, evaluated by comparing the results obtained with the FVM-SLW solver to those obtained with the MC-LBL solver on each wall, the ground and the sky boundary.

Number of gray gases	MAE $[\mathrm{W.m^{-2}}]$	RMSE $[\mathrm{W.m^{-2}}]$
5	0.36	0.46
10	0.35	0.45
15	0.35	0.46

Table 2: Mean absolute errors (MAE) and root-mean-square errors (RMSE) on the volumetric radiative powers for different numbers of gray gases, evaluated by comparing the results obtained with the FVM-SLW solver to those obtained with the MC-LBL solver in the street canyon.

Number of gray gases	MAE $[\mathrm{W.m^{-3}}]$	RMSE $[\mathrm{W.m^{-3}}]$
5	0.16	0.27
10	0.10	0.24
15	0.10	0.22

this figure, the deviations are negligible everywhere except on the top half of the walls A and B and at the center of the ground (where, however, they do not exceed 1 $\mathrm{W.m^{-2}}$). Thus, the FVM-SLW method with the proposed discretization features is able to simulate accurately the longwave net fluxes on the canyon surfaces along with the volumetric radiative powers in the urban air (not shown on the figure), whatever the situation treated (gray or spectral sky with non-gray participating urban air). Therefore, the sky boundary condition constructed with the help of the ALBDF of Equation 6 allows representing correctly the spectral coupling between the sky downward radiation and the urban air. Moreover, on each boundary, the spatial pattern of the deviations from MC-LBL results is the same whatever the case treated, so that the differences between cases can still be assessed accurately with the FVM-SLW results, the deviations compensating each other.

4. Errors on the heat fluxes in the street canyon associated to the assumption of a transparent urban air

It is well known that the street geometry has a significant impact on radiative transfer and the thermal behavior of urban areas [4, 5]. Therefore, using the FVM-SLW model described in Section 3, a range of canyon geometries was studied with the aim of evaluating the errors made on the surface heat fluxes in the street canyon for rather open to compact urban zones, when assuming a transparent urban air. The parameter linked to the canyon geometry studied is the aspect ratio (H/W) of the canyon. The height H of the building is kept constant (*i.e.* 21 m) while the width W of the street canyon is adjusted to reach a given H/W ratio. In this section, the mean difference in the net longwave flux on each wall, noted $\Delta\Phi_\mathrm{w}$, is evaluated by comparing the mean flux obtained in the usual transparent case (Case 1) to the one obtained from the case with participating air and spectral sky (Case 3), taken as the reference case:

$$\Delta\Phi_\mathrm{w} = \overline{\Phi_\mathrm{w,trans}} - \overline{\Phi_\mathrm{w,ref}} \tag{8}$$

where subscript "trans" refers to the transparent case (Case 1) and subscript "ref" refers to the reference case (Case 3), and the spatial average of the net fluxes on each wall are considered.

Table 3 summarizes these differences for the street canyon walls, obtained for H/W ratios of 0.75 (rather open urban zone), 1.5 and 2.4 (compact urban zone). The differences in the net longwave fluxes averaged over each wall increase as the canyon aspect ratio increases. Fluxes absorbed at the walls are 4.0 to 9.2 $\mathrm{W.m^{-2}}$ greater for $H/W = 0.75$ when the urban air is considered transparent, compared with 4.6 to 11.9 $\mathrm{W.m^{-2}}$ greater for $H/W = 2.4$. This can be explained by the fact that the canyon walls have larger sky-view-factors as W increases (and therefore as H/W decreases), receiving in addition a larger share of the flux coming

from the sky and entering through the top of the street (which is unaltered in the urban air) and a smaller share of the flux emitted by the other walls, which limits the impact of the attenuation of these fluxes between the walls. Since most of the attenuation of the radiation from the walls to the other canyon walls takes place over a short distance, the effect of the additional attenuation of this radiation as W increases remains limited compared to the effect of the sky-view-factor. As a result, the differences in the net fluxes tend to diminish as W increases.

Differences are the highest on the coldest faces, *i.e.* the ground and the wall A. Yet, these discrepancies may appear small if no information on the other heat exchange phenomena taking place in the street canyon and their order of magnitude is provided. Consequently, in order to get a better picture of the impact that these differences have on the global heat balance of the walls, and thus on their cooling potential, a simple though realistic convection model was used. The convective heat flux on each wall, noted C_{w}, is modeled using a global value of the convective heat transfer coefficient h_{c}:

$$C_{\mathrm{w}} = h_{\mathrm{c}}(T_{\mathrm{air}} - T_{\mathrm{w}}) \tag{9}$$

The mean total heat flux on each wall is then computed by summing the contributions of the mean net

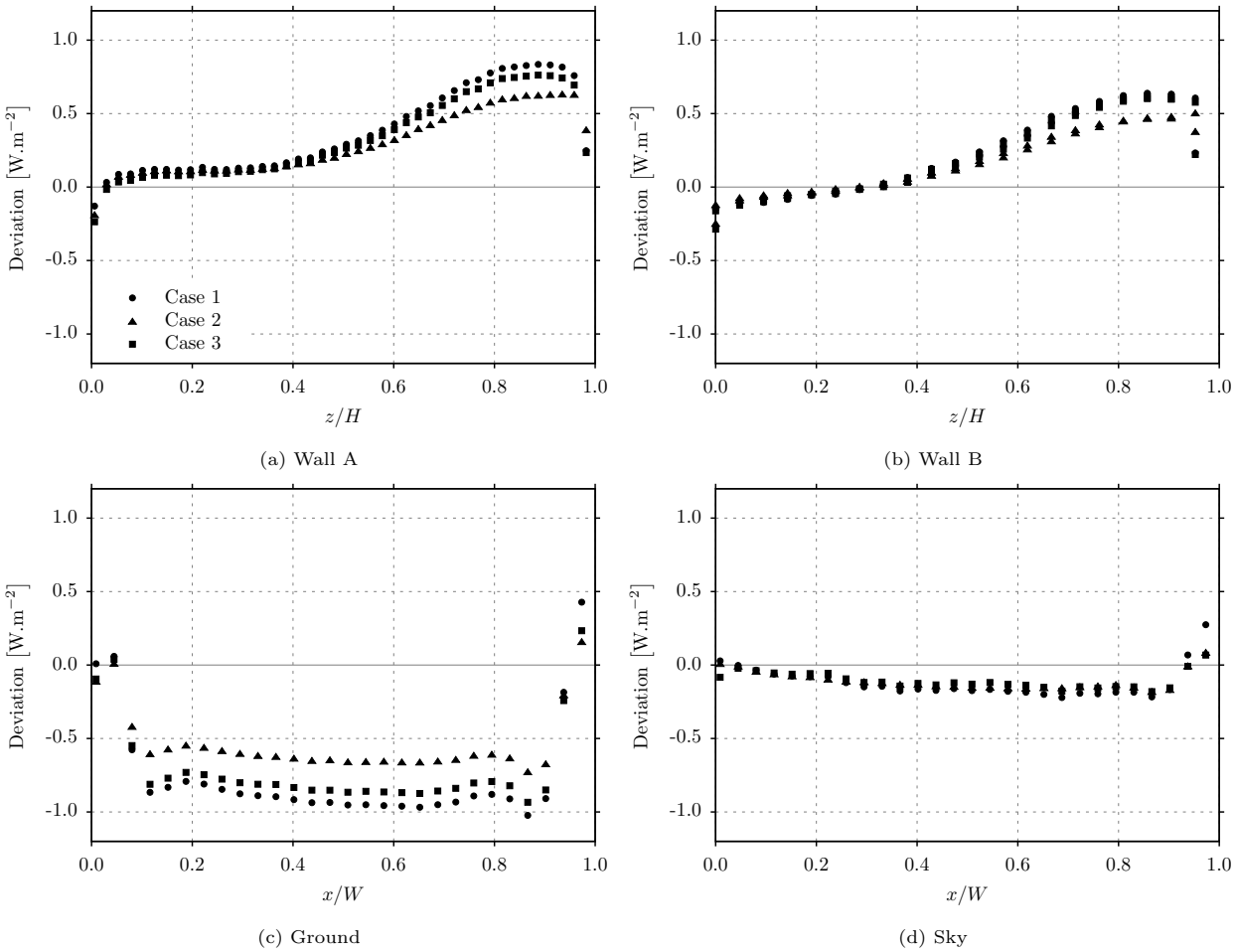

(a) Wall A

(b) Wall B

(c) Ground

(d) Sky

Figure 6: Deviations of the net longwave fluxes calculated by the FVM-SLW solver from those calculated by the MC-LBL solver, on the street canyon walls and at the sky boundary for the three selected cases. The x-axis represents the vertical location for the walls A and B (6a and 6b) and the horizontal location for the ground (6c) and the sky (6d), as defined on Figure 1. Case 1: Transparent - Gray sky, Case 2: Participating - Gray sky, Case 3: Participating - Spectral sky.

Table 3: Differences in the mean net longwave fluxes and in the mean total heat fluxes on each wall of the canyon as a function of the H/W ratio, evaluated by comparing the results obtained in the transparent case (Case 1) with those obtained in the participating case (Case 3, taken as the reference results).

Surface	H/W	LW Net Flux	Total Heat Flux (LW Net + Convective) $h_c = 5$ W.m^{-2}.K^{-1}		$h_c = 20$ W.m^{-2}.K^{-1}	
		$\Delta\Phi_w$ [W.m^{-2}]	Ref. Value [W.m^{-2}]	δ_w	Ref. Value [W.m^{-2}]	δ_w
Ground	0.75	+5.5	-76.6	7.2 %	-135.9	4.1 %
	1.5	+7.2	-48.1	14.9 %	-107.4	6.7 %
	2.4	+7.8	-33.5	23.4 %	-92.7	8.4 %
Wall A	0.75	+9.2	-56.2	16.4 %	-115.4	8.0 %
	1.5	+11.3	-34.2	33.0 %	-93.5	12.1 %
	2.4	+11.9	-20.2	59.0 %	-79.4	15.0 %
Wall B	0.75	+4.0	-174.4	2.3 %	-383.7	1.1 %
	1.5	+4.5	-160.4	2.8 %	-369.7	1.2 %
	2.4	+4.6	-151.6	3.1 %	-360.8	1.3 %

longwave flux and the convective heat flux. The mean relative difference in the total heat flux on each wall (noted δ_w), associated with the assumption of transparent urban air, is computed by dividing the difference in the net longwave flux by the absolute value of the total heat flux in the reference (participating) case:

$$\delta_w = \frac{\Delta\Phi_w}{\overline{\Phi_{w,ref}} + C_w} \tag{10}$$

Table 3 gathers these relative differences for each wall. By setting h_c to a value of 5 W.m^{-2}.K^{-1}, representative of weak wind conditions (with natural convection predominating), the relative difference in the total heat fluxes increases with the aspect ratio H/W and can reach significant values, such as 59 % on the wall A for $H/W = 2.4$. In other words, neglecting the interactions between longwave radiation and the urban air in the street canyon can lead to an underestimation of the cooling rate of the coldest wall by 59 %. For this relatively large aspect ratio, the order of magnitude of the net longwave flux becomes small, so that with limited convective transfer, even a slight difference in the net longwave flux can significantly affect the surface heat balance of the wall. If h_c is fixed at a value of 20 W.m^{-2}.K^{-1}, corresponding to a more intense airflow in the canyon, the relative differences diminish considerably as the convective flux becomes dominant. However, they remain significant, on the order of 4 %−15 % on the wall A and the ground.

Regarding the sky boundary, the mean difference in the net longwave flux, noted $\Delta\Phi_{sky}$, and the mean relative difference, noted δ_{sky}, associated with the assumption of transparent urban air are:

$$\Delta\Phi_{sky} = \overline{\Phi_{sky,trans}} - \overline{\Phi_{sky,ref}} \tag{11}$$

$$\delta_{sky} = \frac{\Delta\Phi_{sky}}{\overline{\Phi_{sky,ref}}} \tag{12}$$

These differences are grouped in Table 4. With differences in the mean leaving flux of around +10 W.m^{-2} for the three aspect ratios, the relative difference in the net fluxes reaches around 7 %. Thus, neglecting the interactions between longwave radiation and the urban air in the street canyon can also lead to an overestimation of the longwave balance of the street canyon by 7 %. This difference may seem small, but is still significant enough not to be overlooked, especially in situations where the cooling of urban zones by longwave radiation is predominant, for example during nighttime when the wind is low.

5. Conclusion

The objective of the present work was to investigate the impact of some assumptions widely used in radiative transfer studies in urban configurations (transparent urban air and gray sky boundary conditions)

Table 4: Differences in the mean net longwave fluxes at the sky boundary ($z/H = 1$) as a function of the H/W ratio, evaluated by comparing the results obtained in the transparent case (Case 1) with those obtained in the participating case (Case 3, taken as the reference results).

H/W	$\Delta\Phi_{\text{sky}}$ $\left[\text{W.m}^{-2}\right]$	Ref. Value $\left[\text{W.m}^{-2}\right]$	δ_{sky}
0.75	+9.8	+137.4	7.1 %
1.5	+10.2	+145.0	7.1 %
2.4	+10.3	+153.2	6.7 %

on the calculation of surface net longwave fluxes and volumetric radiative powers. A preliminary study based on Monte-Carlo Line-by-Line simulations has shown the importance of taking into account the participating character of the air present in the urban canopy layer to avoid overestimation of net fluxes. It has also highlighted that a spectral description of the properties of urban air implies defining spectrally the radiative boundary conditions of the sky in line with the thermo-radiative properties of urban air to account for the strong spectral coupling between downward sky intensity and air absorption.

A faster, though accurate, radiative transfer simulation tool based on the Finite Volume Method and on a full spectrum description of urban air properties (SLW, with 10 gray gases) has been proposed and applied to several street canyons with various aspect ratios. It has been shown that the mean net longwave flux on the coldest walls can be overestimated up to 12 W.m^{-2} in the given configuration when a transparent urban air is considered. This corresponds to a substantial underestimation of the cooling potential of these walls (up to 59 % for a convective heat transfer coefficient of 5 $\text{W.m}^2\text{.K}^{-1}$). As for the mean net longwave flux at the top of the street canyon (*i.e.* at the sky boundary), it can be overestimated by 7 % regardless of the street aspect ratio.

Further study should be carried out to assess the impact of these common assumptions on the nighttime cooling potential of cities. In particular, coupling the model proposed in Section 3 with CFD tools would enable a detailed assessment of the effect of radiation on global energy balances and on the structure of airflow, whose buoyancy forces may be altered by volumetric radiative powers. Particular attention should be paid to the definition of the thermo-physical properties of air and the boundary conditions at the top of the urban canopy layer. In the present work, the atmospheric profiles that led to these definitions were fixed (Mid-Latitude Summer profiles). But in the case of a coupled dynamic simulation, the thermo-physical properties of the atmosphere - mainly temperature fields - cannot be defined in advance, and one of the challenges will be to match the spectral representations of the air and sky boundary conditions to the simulated quantities, while guaranteeing a continuity of downward intensities at the top of the urban canopy layer.

Acknowledgments

This work was supported by the Lyon Urban School which benefited from the financial support of the French National Research Agency (ANR) in the framework of the program "Investissements d'avenir: Instituts Convergences" No. ANR-17-CONV-0004.

References

[1] T. R. Oke, Boundary Layer Climates, 2nd Edition, Routledge, 1987.
[2] H. Cleugh, S. Grimmond, Chapter 3 - Urban Climates and Global Climate Change, in: A. Henderson-Sellers, K. McGuffie (Eds.), The Future of the World's Climate (Second Edition), Elsevier, Boston, 2012, pp. 47–76. doi:10.1016/B978-0-12-386917-3.00003-8.
[3] I. D. Stewart, T. R. Oke, Local climate zones for urban temperature studies, Bulletin of the American Meteorological Society 93 (12) (2012) 1879–1900. doi:10.1175/BAMS-D-11-00019.1.
[4] I. D. Stewart, T. R. Oke, E. S. Krayenhoff, Evaluation of the 'local climate zone' scheme using temperature observations and model simulations, International Journal of Climatology 34 (4) (2014) 1062–1080. doi:10.1002/joc.3746.
[5] T. R. Oke, G. Mills, A. Christen, J. A. Voogt, Urban Climates, Cambridge University Press, Cambridge, 2017. doi:10.1017/9781139016476.

[6] D. Li, E. Bou-Zeid, Synergistic Interactions between Urban Heat Islands and Heat Waves: The Impact in Cities Is Larger than the Sum of Its Parts, Journal of Applied Meteorology and Climatology 52 (9) (2013) 2051–2064. doi:10.1175/JAMC-D-13-02.1.
[7] J. Paravantis, M. Santamouris, C. Cartalis, C. Efthymiou, N. Kontoulis, Mortality Associated with High Ambient Temperatures, Heatwaves, and the Urban Heat Island in Athens, Greece, Sustainability 9 (4) (2017) 606. doi:10.3390/su9040606.
[8] M. Santamouris, Recent progress on urban overheating and heat island research. Integrated assessment of the energy, environmental, vulnerability and health impact. Synergies with the global climate change, Energy and Buildings 207 (2020) 109482. doi:10.1016/j.enbuild.2019.109482.
[9] M. Santamouris, On the energy impact of urban heat island and global warming on buildings, Energy and Buildings 82 (2014) 100–113. doi:10.1016/j.enbuild.2014.07.022.
[10] M. J. Best, C. S. B. Grimmond, Key Conclusions of the First International Urban Land Surface Model Comparison Project, Bulletin of the American Meteorological Society 96 (5) (2015) 805–819. doi:10.1175/BAMS-D-14-00122.1.
[11] N. Lauzet, B. Morille, T. Leduc, M. Musy, What is the Required Level of Details to Represent the Impact of the Built Environment on Energy Demand?, Sustainable synergies from Buildings to the Urban Scale 38 (2017) 611–618. doi:10.1016/j.proenv.2017.03.140.
[12] N. Nazarian, E. S. Krayenhoff, B. Bechtel, D. M. Hondula, R. Paolini, J. Vanos, T. Cheung, W. T. L. Chow, R. de Dear, O. Jay, J. K. W. Lee, A. Martilli, A. Middel, L. K. Norford, M. Sadeghi, S. Schiavon, M. Santamouris, Integrated Assessment of Urban Overheating Impacts on Human Life, Earth's Future 10 (8) (2022). doi:10.1029/2022EF002682.
[13] C. S. B. Grimmond, M. Blackett, M. J. Best, J. Barlow, J.-J. Baik, S. E. Belcher, S. I. Bohnenstengel, I. Calmet, F. Chen, A. Dandou, K. Fortuniak, M. L. Gouvea, R. Hamdi, M. Hendry, T. Kawai, Y. Kawamoto, H. Kondo, E. S. Krayenhoff, S.-H. Lee, T. Loridan, A. Martilli, V. Masson, S. Miao, K. Oleson, G. Pigeon, A. Porson, Y.-H. Ryu, F. Salamanca, L. Shashua-Bar, G.-J. Steeneveld, M. Tombrou, J. Voogt, D. Young, N. Zhang, The International Urban Energy Balance Models Comparison Project: First Results from Phase 1, Journal of Applied Meteorology and Climatology 49 (6) (2010) 1268–1292. doi:10.1175/2010JAMC2354.1.
[14] D. L. Verseghy, D. S. Munro, Sensitivity studies on the calculation of the radiation balance of urban surfaces: II. Longwave radiation, Boundary-Layer Meteorology 48 (1-2) (1989) 1–18. doi:10.1007/BF00121780.
[15] R. J. Hogan, Flexible Treatment of Radiative Transfer in Complex Urban Canopies for Use in Weather and Climate Models, Boundary-Layer Meteorology 173 (1) (2019) 53–78. doi:10.1007/s10546-019-00457-0.
[16] R. Schoetter, C. Caliot, T.-Y. Chung, R. J. Hogan, V. Masson, Quantification of Uncertainties of Radiative Transfer Calculation in Urban Canopy Models, Boundary-Layer Meteorology (2023). doi:10.1007/s10546-023-00827-9.
[17] F. Wang, Modelling of urban micro-climates forbuilding applications : A non-transparentradiative transfer approach, Ph.D. thesis, Université de Lyon (2021).
[18] L. Soucasse, P. Rivière, A. Soufiani, S. Xin, P. Le Quéré, Transitional regimes of natural convection in a differentially heated cubical cavity under the effects of wall and molecular gas radiation, Physics of Fluids 26 (2) (2014) 024105. doi:10.1063/1.4864265.
[19] L. Soucasse, P. Rivière, A. Soufiani, Natural convection in a differentially heated cubical cavity under the effects of wall and molecular gas radiation at Rayleigh numbers up to 3×109, International Journal of Heat and Fluid Flow 61 (2016) 510–530. doi:10.1016/j.ijheatfluidflow.2016.06.012.
[20] T. Kogawa, J. Okajima, A. Sakurai, A. Komiya, S. Maruyama, Influence of radiation effect on turbulent natural convection in cubic cavity at normal temperature atmospheric gas, International Journal of Heat and Mass Transfer 104 (2017) 456–466. doi:10.1016/j.ijheatmasstransfer.2016.08.059.
[21] I. Gordon, L. Rothman, R. Hargreaves, R. Hashemi, E. Karlovets, F. Skinner, E. Conway, C. Hill, R. Kochanov, Y. Tan, P. Wcisło, A. Finenko, K. Nelson, P. Bernath, M. Birk, V. Boudon, A. Campargue, K. Chance, A. Coustenis, B. Drouin, J. Flaud, R. Gamache, J. Hodges, D. Jacquemart, E. Mlawer, A. Nikitin, V. Perevalov, M. Rotger, J. Tennyson, G. Toon, H. Tran, V. Tyuterev, E. Adkins, A. Baker, A. Barbe, E. Canè, A. Császár, A. Dudaryonok, O. Egorov, A. Fleisher, H. Fleurbaey, A. Foltynowicz, T. Furtenbacher, J. Harrison, J. Hartmann, V. Horneman, X. Huang, T. Karman, J. Karns, S. Kassi, I. Kleiner, V. Kofman, F. Kwabia–Tchana, N. Lavrentieva, T. Lee, D. Long, A. Lukashevskaya, O. Lyulin, V. Makhnev, W. Matt, S. Massie, M. Melosso, S. Mikhailenko, D. Mondelain, H. Müller, O. Naumenko, A. Perrin, O. Polyansky, E. Raddaoui, P. Raston, Z. Reed, M. Rey, C. Richard, R. Tóbiás, I. Sadiek, D. Schwenke, E. Starikova, K. Sung, F. Tamassia, S. Tashkun, J. Vander Auwera, I. Vasilenko, A. Vigasin, G. Villanueva, B. Vispoel, G. Wagner, A. Yachmenev, S. Yurchenko, The HITRAN2020 molecular spectroscopic database, Journal of Quantitative Spectroscopy and Radiative Transfer 277 (2022) 107949. doi:10.1016/j.jqsrt.2021.107949.
[22] G. P. Anderson, S. A. Clough, F. X. Kneizys, J. H. Chetwynd, E. P. Shettle, AFGL atmospheric constituent profiles (0.120km), Tech. Rep. AFGL-TR-86-0110, Air Force Geophysics Laboratory, Hanscom AFB, Massachusetts (1986).
[23] R. Nahon, J. Acuña Paz y Miño, B. Beckers, Exploring the sky longwave radiance distribution in the french basque country, in: Proceedings of Building Simulation 2019: 16th Conference of IBPSA (Rome, Italy, Sept. 2-4, 2019), 2019, pp. 4134–4140. doi:10.26868/25222708.2019.210351.
[24] L. J. Dorigon, G. Duciak, R. Brittes, F. Cassol, M. Galarça, F. H. R. França, Wsgg correlations based on hitemp2010 for computation of thermal radiation in non-isothermal, non-homogeneous h2o/co2 mixtures, International Journal of Heat and Mass Transfer 64 (2013) 863–873. doi:10.1016/j.ijheatmasstransfer.2013.05.010.
[25] F. Cassol, R. Brittes, F. H. R. França, O. A. Ezekoye, Application of the weighted-sum-of-gray-gases model for media composed of arbitrary concentrations of h2o, co2 and soot, International Journal of Heat and Mass Transfer 79 (2014) 796–806. doi:10.1016/j.ijheatmasstransfer.2014.08.032.
[26] M. F. Modest, The weighted-sum-of-gray-gases model for arbitrary solution methods in radiative transfer, Journal of Heat Transfer 113 (3) (1991) 650–656. doi:10.1115/1.2910614.

[27] M. F. Modest, S. Mazumder, Radiative Heat Transfer, 4th Edition, Academic Press, 2021.
[28] M. K. Denison, B. W. Webb, An absorption-line blackbody distribution function for efficient calculation of total gas radiative transfer, Journal of Quantitative Spectroscopy and Radiative Transfer 50 (5) (1993) 499–510. doi:10.1016/0022-4073(93)90043-H.
[29] V. P. Solovjov, B. W. Webb, Global spectral methods in gas radiation: The exact limit of the slw model and its relationship to the adf and fsk methods, Journal of Heat Transfer 133 (4) (2011) 042701. doi:10.1115/1.4002775.
[30] V. P. Solovjov, F. Andre, D. Lemonnier, B. W. Webb, The generalized slw model, Journal of Physics: Conference Series 676 (2016) 012022. doi:10.1088/1742-6596/676/1/012022.
[31] V. P. Solovjov, F. Andre, D. Lemonnier, B. W. Webb, The rank correlated slw model of gas radiation in non-uniform media, Journal of Quantitative Spectroscopy and Radiative Transfer 197 (2017) 26–44. doi:10.1016/j.jqsrt.2017.01.034.
[32] V. P. Solovjov, B. W. Webb, F. Andre, The rank correlated fsk model for prediction of gas radiation in non-uniform media, and its relationship to the rank correlated slw model, Journal of Quantitative Spectroscopy and Radiative Transfer 214 (2018) 120–132. doi:10.1016/j.jqsrt.2018.04.026.
[33] V. P. Solovjov, B. W. Webb, F. André, D. Lemonnier, Locally correlated slw model for prediction of gas radiation in non-uniform media and its relationship to other global methods, Journal of Quantitative Spectroscopy and Radiative Transfer 245 (2020) 106857. doi:10.1016/j.jqsrt.2020.106857.
[34] V. P. Solovjov, B. W. Webb, F. Andre, Radiative Properties of Gases, in: Handbook of Thermal Science and Engineering, Springer International Publishing, 2018, pp. 1069–1141. doi:10.1007/978-3-319-26695-4_59.
[35] B. W. Webb, V. P. Solovjov, F. André, Chapter Four - The spectral line weighted-sum-of-gray-gases (SLW) model for prediction of radiative transfer in molecular gases, in: E. M. Sparrow, J. P. Abraham, J. M. Gorman, W. J. Minkowycz (Eds.), Advances in Heat Transfer, Vol. 51 of Advances in Heat Transfer, Elsevier, 2019, pp. 207–298. doi:https://doi.org/10.1016/bs.aiht.2019.08.003.
[36] F. André, V. P. Solovjov, B. W. Webb, The ω-absorption line distribution function for rank correlated slw model prediction of radiative transfer in non-uniform gases, Journal of Quantitative Spectroscopy and Radiative Transfer 280 (2022) 108081. doi:10.1016/j.jqsrt.2022.108081.
[37] J.-L. Consalvi, F. Nmira, F. André, V. P. Solovjov, B. W. Webb, A simplified ω-aldf rank-correlated full-spectrum k-distribution model for combustion applications, Journal of Quantitative Spectroscopy and Radiative Transfer 322 (2024) 109034. doi:10.1016/j.jqsrt.2024.109034.
[38] F. Andre, V. Solovjov, D. Lemonnier, B. Webb, Comonotonic global spectral models of gas radiation in non-uniform media based on arbitrary probability measures, Applied Mathematical Modelling 50 (2017) 741–754. doi:10.1016/j.apm.2017.05.033.
[39] J. C. Chai, H. S. Lee, S. V. Patankar, Finite volume method for radiation heat transfer, Journal of thermophysics and heat transfer 8 (3) (1994) 419–425. doi:10.2514/3.559.
[40] P. J. Coelho, Advances in the discrete ordinates and finite volume methods for the solution of radiative heat transfer problems in participating media, Journal of Quantitative Spectroscopy and Radiative Transfer 145 (2014) 121–146. doi:10.1016/j.jqsrt.2014.04.021.
[41] S. H. Kim, K. Y. Huh, A new angular discretization scheme of the finite volume method for 3-D radiative heat transfer in absorbing, emitting and anisotropically scattering media, International Journal of Heat and Mass Transfer 43 (7) (2000) 1233–1242. doi:10.1016/S0017-9310(99)00211-2.